energies

MDPI

Article

A Chaos-Embedded Gravitational Search Algorithm for the Identification of Electrical Parameters of Photovoltaic Cells

Arturo Valdivia-González *, Daniel Zaldívar, Erik Cuevas, Marco Pérez-Cisneros, Fernando Fausto * and Adrián González

Departamento de Electrónica, Universidad de Guadalajara, CUCEI Av. Revolución 1500, 44430 Guadalajara, Mexico; daniel.zaldivar@cucei.udg.mx (D.Z.); erik.cuevas@cucei.udg.mx; (E.C.); marco.perez@cucei.udg.mx (M.P.-C.); shyru00@hotmail.com (A.G.)

* Correspondence: arturo.vg7@gmail.com (A.V.-G.); neosbreak@gmail.com (F.F.); Tel.: +52-33-1378-5900 (ext. 7715) (A.V.-G.)

Received: 24 April 2017; Accepted: 7 July 2017; Published: 21 July 2017

Abstract: Solar energy is used worldwide to alleviate the daily increasing demands for electric power. Photovoltaic (PV) cells, which are used to convert solar energy into electricity, can be represented as equivalent circuit models, in which a series of electrical parameters must be identified in order to determine their operating characteristics under different test conditions. Intelligent approaches, like those based in population-based optimization algorithms like Particle Swarm Optimization (PSO), Genetic Algorithms (GAs), and Simulated Annealing (SA), have been demonstrated to be powerful methods for the accurate identification of such parameters. Recently, chaos theory have been highlighted as a promising alternative to increase the performance of such approaches; as a result, several chaos-based optimization methods have been devised to solve many different and complex engineering problems. In this paper, the Chaotic Gravitational Search Algorithm (CGSA) is proposed to solve the problem of accurate PV cell parameter estimation. To prove the feasibility of the proposed approach, a series of comparative experiments against other similar parameters extraction methods were performed. As shown by our experimental results, our proposed approach outperforms all other methods compared in this work, and proves to be an excellent alternative to tackle the challenging problem of solar cell parameters identification.

Keywords: solar cell; parameters identification; chaotic gravitational search algorithm; population-based algorithm

1. Introduction

In recent years, several economic and environmental phenomenon, such as the non-stopping increase on the cost of fossil fuel along with its probable depletion in the near future, the dramatic increase on the air pollution, and the ever worrying climatic changes and global warming effect, have motivated an increasing trend on the use of renewable energy sources [1].

Solar energy is one of the most practical alternative energy sources, with it being used worldwide to alleviate the daily increasing demands for electric power [2]. Typically, photovoltaic (PV) cells are used to convert solar energy into electric power. PV cells (also called solar cells) are different from most conventional energy sources due to the fact that they are free of pollutant emissions, making them an environmental-friendly source of energy. In addition, solar energy has the all-important advantage of being a practically inexhaustible source of energy, which further makes PV systems an even more promising source of power [3].

While currently subjected to many challenges, such as variations on electric power generation, life duration, and economic feasibility, PV technologies are expected to become one of the most important renewable energy sources of the planet. In fact, it is known that solar PV is currently the fastest growing power-generation technology in the world, with a reported annual growth rate of 50% just between 2005 and 2013. Such a rapid increase in the use of PV systems, along with the growing demand for electric power has evocated the necessity of research oriented to maximizing the performance of such power generation technologies [2].

Typically, the behavior of PV cells may be characterized by its current vs. voltage (I-V) output curves. Such I-V characteristics are used to model the performance of PV cells under a set of specific operating conditions, such as irradiance level and environmental temperature. Usually, PV cell manufacturers provide datasheets containing limited tabular data measured by considering a set of standard test conditions [4]. However, it is known that PV systems often operate in environments which conditions are completely different than those of the standard test conditions (STC), and as such the available data usually fails to meet the engineering requirements [3].

Given that the performance of PV cells (and by extension, PV systems) is entirely dependent on the environmental conditions in which these are meant to operate, it is clear that there is a necessity for accurate, yet practical models that could help to predict the performance of such power generation systems under many different operating conditions. As a result of such engineering necessities, numerous modeling approaches have been proposed to accurately model the behavior of PV cells. Among them, there are two particular PV cell models that are commonly used in practice: the single-diode model, and the double-diode model [5]. Both of these approaches model PV cells as diode-resistance equivalent circuits in which a particular set of electrical parameters may be identified. Such parameters includes the cell's photogenerated current, saturation current, series resistance, shunt resistance and diode ideality factor [5,6]. The main problem, however, is to identify the optimal parameter values which, when applied to a selected model, produce the best possible approximation to the experimental data (I-V characteristics) obtained from a particular PV cell.

Typically, deterministic-based approaches, such as the Newton-Rhapson methods or Lambert-W functions [7], are applied in the identification of PV cell parameters due to their simplicity and notoriously good convergence speed. However, these methods are known to be extremely reliant upon several model restrictions, such as convexity and differentiability, which further limit their application [8]. In addition, the non-linear, multi-variable and multi-modal nature of the PV cell parameter identification problem makes it more difficult for deterministic methods to accurately find a feasible solution due to the fact they are highly sensitive to both the location of the initial solution and the possibility of falling into local optima [2].

Recently, the use of heuristic-based approaches (also referred as intelligent approaches) have been identified as a promising alternative to the use of deterministic techniques when solving complex engineering problems. In particular, evolutionary algorithms (EAs), which propose innovative and interesting artificial intelligence schemes, have been successfully applied to find accurate solutions for a wide variety of engineering applications, such as mechanical design, data analysis, communications, computer vision, energy management, among others. In fact, many of these evolutionary optimization methods have been reported in the literature as viable alternatives to solve the all-important problem of PV cell parameter identification [2,9–12]. Some of these methods include well-known state-of-the art approaches such as Particle Swarm Optimization (PSO) [9,13], Artificial Bee Colony (ABC) [2,14], Genetic Algorithms (GAs) [11,15], Differential Evolution (DE) [10,16], Simulated Annealing (SA) [17], Harmony Search (HS) [11,18], Gravitational Search Algorithm (GSA) [19,20], among others.

However, although many of these EA-based approaches have demonstrated to have a significantly higher performance in comparison to classic deterministic techniques, they are also known to have important limitations. In the case of PSO and GA, for example, the use elitism-based operators in the exploration of the feasible solutions space results in a tendency to concentrate search agents toward possible local optima, often forcing a premature convergence. On the other hand, single-searcher methods such as SA and HS are known for being extremely sensitive to their starting search point, especially when dealing with highly multi-modal problems [2,8,9].

Recently, chaos theory have received a significant degree of attention as an alternative to improve the performance of EA methods. As shown by several works in the literature, integrating chaotic behaviors into population-based optimization approaches allows to substantially improve the exploration and exploitation properties of search agents [21–24]. With that being said, many recently proposed chaos-based optimization approaches have been successfully applied to solve a wide variety of complex and challenging engineering problems [24].

In this paper the Chaotic Gravitational Search Algorithm (CGSA) [24] is proposed for solving the problem of accurate PV cell parameters estimation. Like GSA, in CGSA search agents are represented as individual masses, which movement within a feasible search space is governed by a set of evolutionary operators inspired in the laws of gravity and motion [19]. Unique to CGSA, however, is the integration of several chaotic behaviors used to "chaotically" modify the intensity of the gravitational forces which allows masses to move within the feasible search space. As demonstrated by [24], integration chaos into CGSA yield to a significantly better performance, surpassing not only its original counterpart, but also many other state-of-the-art optimization methods. In order to verify the feasibility of the proposed GCSA-based approach, it is compared with several other similar solar cell parameters extraction methods in terms of performance. The remainder of this paper is organized as follows: in Section 2, the theory behind the modeling of PV cells is presented. In Section 3, the key traits of the CGSA method are exposed. In Section 4, our experimental results are presented. Finally, in Section 5, our conclusions are drawn.

2. Model of a Photovoltaic Cell

A PV cell is a semiconductor device which is able to convert the light irradiated from the Sun into electricity. This energy conversion phenomenon occurs by means of the so called photovoltaic effect [5]. In practice, the electrical behavior of a PV cell is described by its I-V curves, measured by considering a particular set of operating conditions. Typically, PV cell manufacturers provide datasheets which include several electrical and thermal operating characteristics, measured by considering a set of typical standard test conditions (STC). However, as illustrated in Section 1, one of the main problems related to the implementation of PV systems is the difficulty for predicting the behavior of PV cells under many different operating condition. As a result of the necessity for reliable tools which could help to predict the behavior of PV cells under such varying environmental conditions, several parametric models have been described in literature. In this section, we will analyze some of the most widely accepted models used for the characterization of PV cells.

2.1. Ideal Model of a PV Cell

Ideally, a PV cell is considered to be electrically equivalent to a current source connected in parallel with a diode (see Figure 1) [5]. In such a model the solar cell's current is given by the following equation:

$$I_{\mathrm{cell}} = I_{\mathrm{L}} - I_{\mathrm{D}} \tag{1}$$

where I_{L} denotes the light-generated current (also called photocurrent) of the PV cell, while I_{D} stands for the current circulating through diode D. Furthermore, the diode's current I_{D} is modeled in terms of the Shockley diode equation as:

$$I_{\mathrm{D}} = I_0 \left[\exp\left(\frac{q \cdot V_{\mathrm{D}}}{n \cdot k \cdot T_c} \right) - 1 \right] \tag{2}$$

where I_0 and V_{D} represent the reverse saturation current (or dark current) and the voltage across diode D, respectively. Furthermore, the value $q = 1.602 \times 10^{19}$ C (Coulombs) represents the electron charge, while $k = 1.38065 \times 10^{23}$ J/K stands for the Boltzmann constant. Also, T_c stands for the temperature of the PV cell in Kelvin (K). Finally, the value n stands for the diode ideality factor, which represents how close the diode D follows the behavior of an ideal diode.

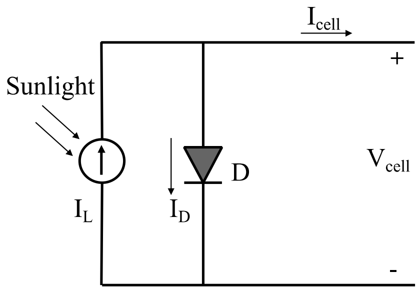

Figure 1. Ideal circuit model of a photovoltaic cell.

As shown in Figure 1, the ideal cell's output voltage correspond to the voltage across the diode D (that is, $V_{\text{cell}} = V_{\text{D}}$). With that being said, and by replacing the term I_{D} given by Equation (2) into Equation (1), the PV cell's current is then given as:

$$I_{\text{cell}} = I_{\text{L}} - I_0 \left[\exp\left(\frac{q \cdot V_{\text{cell}}}{n \cdot k \cdot T_c} \right) - 1 \right] \tag{3}$$

As illustrated by Equation (3), the ideal PV cell model has three unknown parameters that has be identified: the photocurrent I_{L}, the reverse saturation current I_0 and the diode ideality factor n. This three parameters model is also referred in the literature as the 3-p model and is commonly uses to describe the fundamental operating principles of solar cells [5].

2.2. Single-Diode Model

While the ideal solar cell model (or 3-p model) is useful to illustrate the basic electrical principles which govern the behavior of a PV cell, it is usually not used to simulate real cell operating conditions due to the fact that its accuracy is compromised by several limitations commonly found in practice. For example, solar cells are known to be subject to a series of power losses related to the metal grid's resistance, contacts and current-collecting wires [5,6]. To represent such resistive losses a lumped resistor R_{s} may be added to the ideal circuit model, as illustrated in Figure 2.

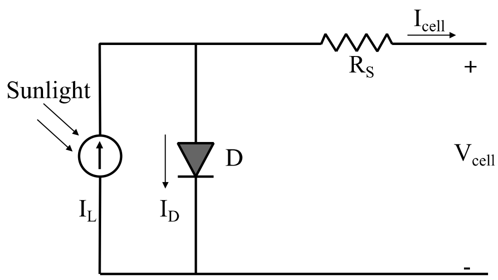

Figure 2. Single-Diode model of a photovoltaic cell, showing the added lumped series resistor R_{s}.

By considering the addition of the lumped resistor R_{s}, the current I_{D} which circulates through the diode D is now be given by the following expression:

$$I_{\text{D}} = I_0 \left[\exp\left(\frac{q(V_{\text{cell}} + I_{\text{cell}} \cdot R_{\text{s}})}{n \cdot k \cdot T_c} \right) - 1 \right] \tag{4}$$

Then, by replacing Equation (4) in Equation (1), the PV cell's net current flow I_{cell} is now given as:

$$I_{\text{cell}} = I_{\text{L}} - I_0 \left[\exp\left(\frac{q(V_{\text{cell}} + I_{\text{cell}} \cdot R_{\text{s}})}{n \cdot k \cdot T_c} \right) - 1 \right] \tag{5}$$

In addition, a series of shunt resistive losses, typically caused as a result of certain PV cell manufacturing defects, are also known to take place when PV cells are operating. This kind of resistive losses are usually represented by adding a resistor R_{p} in parallel to the ideal cell model [5]. Figure 3 shows the equivalent PV cell circuit model which includes both, the lumped resistor R_{s} and the shunt resistor R_{p}.

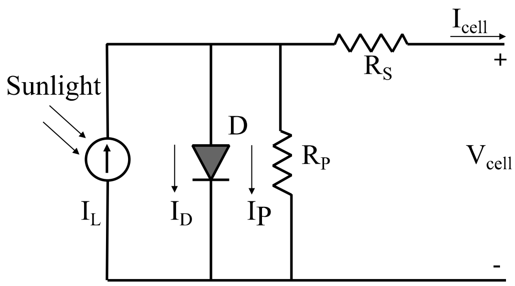

Figure 3. Single-diode model of a photovoltaic cell, which includes both a lumped series resistor R_{s} and a shunt resistor R_{p}.

With the addition of such shunt resistance the solar cell's current flow I_{cell} may now be modeled by the following equation:

$$I_{\mathrm{cell}} = I_{\mathrm{L}} - I_{\mathrm{D}} - I_{\mathrm{p}} \tag{6}$$

where I_{p} denotes the current flowing through the shunt resistor R_{p}, as given as:

$$I_{\mathrm{p}} = \frac{V_{\mathrm{cell}} + I_{\mathrm{cell}} \cdot R_{\mathrm{s}}}{R_{\mathrm{p}}} \tag{7}$$

Then, from Equation (5), the cell's current flow I_{cell} is finally given as:

$$I_{\mathrm{cell}} = I_{\mathrm{L}} - I_0 \left[\exp\left(\frac{q(V_{\mathrm{cell}} + I_{\mathrm{cell}} \cdot R_{\mathrm{s}})}{n \cdot k \cdot T_c} \right) - 1 \right] - \frac{V_{\mathrm{cell}} + I_{\mathrm{cell}} \cdot R_{\mathrm{s}}}{R_{\mathrm{p}}} \tag{8}$$

As evidenced by Equation (8), in addition to the three unknown parameters of the ideal PV cell model (photocurrent I_{L}, dark current I_0 and diode ideality factor n), two extra parameters must be identified in this modified single-diode model, namely the values of both, the lumped resistor R_{s} and the shunt resistor R_{p}. This modified single-diode model is also known in the literature as the 5-p model, and is one of the most widely used approaches for modeling the behavior of PV cells [5,6].

2.3. Double-Diode Model

Although single-diode models are known to give an acceptable approximation to the behavior of practical solar cells, there are other considerations that must be taken into account in order to achieve higher degrees of accuracy. Particularly, the photocurrent in a solar cell is not generated only by a single diode. In fact, the output current of a PV cell is more accurately modeled as a linear superposition of both, charge and diffusion effects, corresponding to multiple elementary diodes, consistently distributed along space-charge region of the solar cell [6]. As such, a more adequate representation of a PV cell's equivalent circuit is achieved by considering two Shockley diodes, D_1 and D_2, in parallel to a current source and its respective lumped and shunt resistor R_{s} and R_{p}, respectively, as shown in Figure 4 [5]. In such equivalent circuit, the PV cell's output current is given by the following equation:

$$I_{\mathrm{cell}} = I_{\mathrm{L}} - I_{\mathrm{D1}} - I_{\mathrm{D2}} - I_{\mathrm{p}} \tag{9}$$

where I_{D1} and I_{D2} represent the current which circulates thought the diodes D_1 and D_2, respectively. From Equation (4), we may represent both I_{D1} and I_{D2} with the following expressions:

$$I_{\text{D1}} = I_{01}\left[\exp\left(\frac{q(V_{\text{cell}} + I_{\text{cell}} \cdot R_{\text{s}})}{n_1 \cdot k \cdot T_c}\right) - 1\right] \tag{10}$$

$$I_{\text{D2}} = I_{02}\left[\exp\left(\frac{q(V_{\text{cell}} + I_{\text{cell}} \cdot R_{\text{s}})}{n_2 \cdot k \cdot T_c}\right) - 1\right] \tag{11}$$

where I_{01} and I_{02} denote the reverse saturation currents corresponding to the diodes D_1 and D_2, respectively. Furthermore, n_1 and n_2, respectively, stand for the diode ideality factors for D_1 and D_2. Finally, R_{s} stand for the value of the Double-Diode model's lumped resistor, as illustrated in Figure 4.

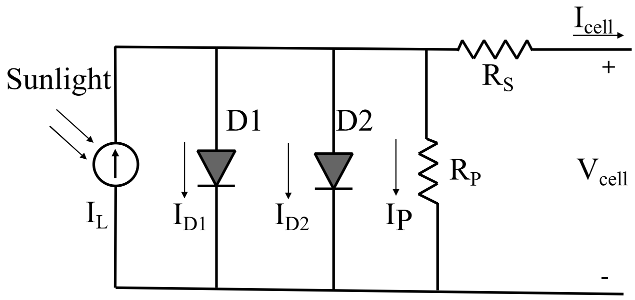

Figure 4. Double-diode model of a photovoltaic cell.

Lastly, by replacing Equations (10) and (11), along with the term I_{p} as given by Equation (7), the expression which describes the PV cell's net current flow I_{cell} is finally given as:

$$I_{\text{cell}} = I_{\text{l}} - I_{01}\left[\exp\left(\frac{q(V_{\text{cell}}+I_{\text{cell}} \cdot R_{\text{s}})}{n_1 \cdot k \cdot T_c}\right) - 1\right] - I_{02}\left[\exp\left(\frac{q(V_{\text{cell}}+I_{\text{cell}} \cdot R_{\text{s}})}{n_2 \cdot k \cdot T_c}\right) - 1\right] - \frac{V_{\text{cell}}+I_{\text{cell}} \cdot R_{\text{s}}}{R_{\text{p}}} \tag{12}$$

As shown in Equation (12), in the double-diode model, there exist a total of seven unknown parameters that are required to be identified: the solar cell's photocurrent (I_{L}), the diodes' reverse saturation currents (I_{01} and I_{02}), the diodes' ideality factors (n_1 and n_2), and the values of the lumped and shunt resistors (R_{s} and R_{p}, respectively).

3. The Chaotic Gravitational Search Algorithm

The Chaotic Gravitational Search Algorithm (CGSA) [24], is a modified version of the well-known Gravitational Search Algorithm (GSA) proposed by Rashedi et al. in [19]. Like its original counterpart, the CGSA approach is a population-based optimization algorithm, in which, search agents explore a feasible search space guided by a set of movement operators inspired by the laws of gravity and motion. Unique to the CGSA method, however, is the inclusion of several chaotic map functions, embedded into the movement operators of the original GSA. As demonstrated by the authors of [24], the inclusion of such chaotic behaviors are able to drastically improve the exploration and exploitation properties of search agents, and thus, improve the overall performance of the search process. In this section we will analyze the most important traits of both the original GSA approach and the modified CGSA method.

3.1. The Gravitational Search Algorithm

The GSA is a population-based optimization algorithm, in which, the movement of search agents within a feasible search space is guided by a set of unique evolutionary operators based in both the laws of gravitation and motion [19]. In the GSA approach, search agents are represented as a set of N individual masses, whose positions within a feasible n-dimensional search space (also referred as a system) represent a candidate solution for a given optimization problem at a given time t. With that being said, in GSA, the position of a specific mass (search agent) i is given as:

$$\mathbf{x}_i(t) = \left[x_i^1(t), \ldots, x_i^d(t), \ldots x_i^n(t)\right] \text{ for } i = 1, 2, \ldots, N \tag{13}$$

where the elements $x_i^d(t)$ denotes the position of the i-th search agent at the d-th dimension and where t stands for the current time (iteration).

Also, each solution $\mathbf{x}_i(t)$ is assigned with a particular mass value M_i, which magnitude is related to the current fitness of such solution, as expressed by the following equation:

$$M_i(t) = \frac{m_i(t)}{\sum_{J=1}^{N} m_j(t)} \tag{14}$$

where $m_i(t)$ denotes the normalized fitness value related to the i-th agent at a given time t, as given as:

$$m_i(t) = \frac{f_i(t) - f_{\text{worst}}(t)}{f_{\text{best}}(t) - f_{\text{worst}}(t)} \tag{15}$$

where, for a given time t, $f_i(t) = f(\mathbf{x}_i(t))$ denotes the fitness (quality) value resulting from the evaluation i-th candidate solution ($\mathbf{x}_i(t)$) with regard to the target objective function $f(\cdot)$, while $f_{\text{best}}(t)$ and $f_{\text{worst}}(t)$ stand for the current best and worst fitness values at said time t, respectively. Note that for a case of cost function maximization, $f_{\text{best}}(t)$ and $f_{\text{worst}}(t)$ are given by the following expressions:

$$f_{\text{best}}(t) = \max_{i \in \{1,2,\ldots,N\}} (f_i(t)),\ f_{\text{worst}}(t) = \min_{i \in \{1,2,\ldots,N\}} (f_i(t)) \tag{16}$$

On the other hand, if cost function minimization is desired, $f_{\text{best}}(t)$ and $f_{\text{worst}}(t)$ are instead given as:

$$f_{\text{best}}(t) = \min_{i \in \{1,2,\ldots,N\}} (f_i(t)),\ f_{\text{worst}}(t) = \max_{i \in \{1,2,\ldots,N\}} (f_i(t)) \tag{17}$$

In the GSA approach, the mass of an individual may be conceptually differentiated as either active gravitational mass, $M_{ai}(t)$, passive gravitational mass, $M_{pi}(t)$, or inertial mass, $M_{ii}(t)$. In any case, the gravitational and inertial masses of any individual are equally calculated by considering Equation (14), such that:

$$M_{ai}(t) = M_{pi}(t) = M_{ii}(t) = M_i(t) \tag{18}$$

Furthermore, each of these masses are supposed to be in constant interaction with each other as a result of several gravitational forces, experimented by such objects at a specific time instant. Specifically, for a given time (iteration) t the total gravitational force experimented between a particular solution and all other masses in the system is calculated as:

$$F_i^d(t) = \sum_{j=1,\ j \neq i}^{N} \text{rand}_j \cdot F_{ij}^d(t) \tag{19}$$

where rand_j denotes a random number, generated within the interval $(0,1)$. Furthermore, $F_{ij}^d(t)$ denotes the gravitational force acting between a specific pair of agents i and j, as given as:

$$F_{ij}^d(t) = G(t)\frac{M_{pi}(t)\cdot M_{aj}(t)}{R_{ij}(t)+\varepsilon}\left(x_j^d(t) - x_i^d(t)\right) \tag{20}$$

where $M_{aj}(t)$ represents the active gravitational mass corresponding to the j-th search agent, while and $M_{pi}(t)$ stand for the passive gravitational mass related to the i-th agent (see Equations (14) and (16)). Furthermore, $R_{ij}(t) = \|X_i(t), X_j(t)\|_2$ stand for the Euclidian distance between the agents i and j, while the value ε denotes a small constant used to prevent a division by zero (i.e., when the distance between both agents i and j is equal to zero). Finally, the term $G(t)$ is known as gravitational constant [19] and its value is expressed as:

$$G(t) = G_0 \cdot \exp\left(-\alpha\frac{t}{T}\right) \tag{21}$$

with G_0 denoting the gravitational constant's initial value, while α is a constant descending coefficient. Also, the value T stands for the maximum number of iterations (also referred as age of system) which comprises the algorithm's whole evolutionary process.

As a result of these gravitational interactions, masses within a system are also supposed to be accelerated toward a particular direction, thus, experimenting a motion effect. The gravitational acceleration related to each agent within such gravitational system is modeled as:

$$a_i^d(t) = \frac{F_i^d(t)}{M_{ii}^d(t)} \tag{22}$$

where for a given time t, $F_i^d(t)$ denotes the total gravitational force experimented by the i-th search agent at the d-th (see Equation (19)), while $M_{ii}^d(t)$ stands for the inertial mass of said agent i at the dimension d (see Equations (14) and (18)).

The acceleration experimented by the i-th agent at time t is used to figure its velocity for the next time instant. With that being said, the velocity and position of a given search agent at the following iteration of GSA's evolutionary process ($t+1$) is given as:

$$v_i^d(t+1) = \text{rand}_i \cdot v_i^d(t) + a_i^d(t) \tag{23}$$

$$x_i^d(t+1) = x_i^d(t) + v_i^d(t+1) \tag{24}$$

where $v_i^d(t)$ and $x_i^d(t)$ denotes the velocity and position, respectively, of the agent i at the d-th dimension, whereas $a_i^d(t)$ refer to the acceleration experimented by such agent i, as given by Equation (22). Furthermore, rand_i denotes a random number, generated within the interval $(0,1)$.

One important trait that must be emphasized about GSA is the fact that it is a memory-less algorithm. While this may initially seem like disadvantage, the efficiency of the GSA's search strategy has been proven to be comparable (and sometimes better) to that of many of the algorithms which incorporate a memory as a part of their design [19]. In general, the GSA algorithm may be summarized by the following steps:

1. Initialize the systems population (search agents).
2. Evaluate the fitness of each agent and find the best and worst fitness values.
3. Update the gravitational constant $G(t)$ (Equation (19)).
4. Calculate the mass $M_i(t)$ (Equation (14)) and acceleration $a_i(t)$ (Equation (22)) of each agent.
5. Update the velocity $v_i(t)$ (Equation (23)) and position $x_i(t)$ (Equation (24)) of each agent.
6. If the stop criterion is not met, return to Step 2.
7. Return best solution.

3.2. Chaos-Embedded Gravitational Constants for GSA

As previously stated, GSA is an agent-based optimization algorithm which design is inspired by the laws of gravitation and motion [19]. Although the GSA approach has demonstrated excellent performance when compared to other state-of-the-art optimization methods [25–29], it is known to suffer from several problems commonly found in such population-based approaches. In particular, the dependence on the fitness function for calculating the mass of search agents often causes GSA search speed to get deteriorated as agents become heavier, essentially manifesting a slow converge rate which worsens as the iterations increase. In addition, since the movement step of each search agent is also determined by the value taken by the gravitational constant at each iteration, it is required to properly control the way in which such value decreases in order to prevent agents from getting trapped into a local optima [24].

Motivated by these limitations, Mirjalili and Gandomi devised a modified version to the original GSA approach known as Chaotic Gravitational Search Algorithm (CGSA) [24]. In CGSA, chaotic map functions are embedded into the gravitational constant of the original GSA method which, consequently, "chaotically" modify the intensity of the total gravitational force experienced by search agents at each iteration. As such, the modified value for the gravitational constant $G(t)$, as proposed by the CGSA methodology, is given as:

$$G(t) = C^{\text{norm}}(t) + G_0 \cdot \exp\left(-\alpha \frac{t}{T}\right) \tag{25}$$

where the term $G_0 \cdot \exp\left(-\alpha \frac{t}{T}\right)$ stand for the original GSA's gravitational constant value, as illustrated by Equation (21) in Section 3.1. Furthermore, the term $C^{\text{norm}}(t)$ denotes a normalized chaotic map function, which is given as:

$$C^{\text{norm}}(t) = \frac{(C(t) - a) \cdot V(t)}{(b - a)} \tag{26}$$

where $C(t)$ denotes the value mapped by the embedded chaotic function at a given time t (see Appendix A), while the values $[a, b]$ denotes an interval associated with such chaotic function. Furthermore, $V(t)$ denotes the maximum value within the interval $[0, V(t)]$ at which the chaotic function $C(t)$ is desired to be normalized and is given as:

$$V(t) = max - \frac{t}{T}(max - min) \tag{27}$$

with T denoting the algorithm's maximum number of iterations, while the values $[min, max]$ denote a user-defined adaptive interval.

The authors of CGSA studied the effects of embedding several different chaotic maps $C(t)$ into the gravitational constant function of the original GSA (see Appendix A). In fact, it is observed by the authors that, by integrating chaotic behaviors into the movement operators of GSA, agents are given a way to assist themselves to both improve their convergence speed and to avoid being trapped into local optima. With that being said, the inclusion of such random chaotic behaviors greatly improves the balance between exploration and exploitation of solutions and, as a result, deliver a much better performance in comparison to the traditional GSA approach [24].

4. Solar Cell's Parameter Identification as an Optimization Problem

As previously illustrated in Section 2, the main problem concerning to the modeling of PV cells is to accurately identify a set of electrical parameters corresponding to a particular cell model, and such that it allows to produce the best possible approximation to the I-V characteristics of a real solar cell. From an optimization point of view this could be interpreted as a minimization problem in which we aim to minimize the difference between a real cell's I-V measurements and the I-V characteristics calculated by considering a particular set of identified parameters. With that being said, an intuitive way to measure such difference is to consider the root mean squared error (RMSE) with regard to a set on N experimental I-V measurement [2,11], as defined as:

$$\mathrm{RMSE}(\mathbf{x}) = \sqrt{\frac{1}{N}\sum_{i=1}^{N}\left(I_{\mathrm{m}}^{i} - I_{\mathrm{e}}^{i}\left(I_{\mathrm{m}}^{i}, V_{\mathrm{m}}^{i}, \mathbf{x}\right)\right)^{2}} \tag{28}$$

where I_{m}^{i} and V_{m}^{i} each denote the i-th current and voltage measurement (from within the set of N experimental observations), respectively, while $\mathbf{x}$ stand for the set of decision variables (parameters) that are required to be identified. Furthermore, $I_{\mathrm{e}}^{i}\left(V_{\mathrm{m}}^{i}, I_{\mathrm{m}}^{i}, \mathbf{x}\right)$ stands for the estimated PV cell's current with regard to a particular solar cell model and its respective set of parameters $\mathbf{x}$.

As previously described in Section 2, there are several PV cell circuit models which could be considered to estimate the I-V characteristics of solar cells: (1) ideal cell model (see Section 2.1), (2) single-diode (SD) model (see Section 2.2), and (3) double-diode (DD) model (see Section 2.3). While in practice the ideal cell model is usually not applied due to its lack of accuracy, both the SD model and DD model are more commonly considered to simulate the operating characteristics of PV cells [5]. With that being said, for Equation (28), the PV cell's calculate current $I_{\mathrm{e}}^{i}\left(V_{\mathrm{m}}^{i}, I_{\mathrm{m}}^{i}, \mathbf{x}\right)$ with regard to the single-diode (SD) model, as described in Section 2.2, is given from the Equation (8) as:

$$I_{e}^{i}\left(V_{\mathrm{m}}^{i}, I_{\mathrm{m}}^{i}, \mathbf{x}\right) = I_{\mathrm{L}} - I_{0}\left[\exp\left(\frac{q\left(V_{\mathrm{m}}^{i} + R_{\mathrm{s}} \cdot I_{\mathrm{m}}^{i}\right)}{n \cdot k \cdot T_{c}}\right) - 1\right] - \frac{V_{\mathrm{m}}^{i} + R_{\mathrm{s}} \cdot I_{\mathrm{m}}^{i}}{R_{\mathrm{p}}} \tag{29}$$

where $\mathbf{x} = \left[R_{\mathrm{s}}, R_{\mathrm{p}}, I_{\mathrm{L}}, I_{0}, n\right]$ represent the five-parameter decision vector corresponding to the PV cell's SD model [5].

On the other hand, if the double-diode (DD) model described in Section 2.3 is chosen, $I_{\mathrm{e}}^{i}\left(V_{\mathrm{m}}^{i}, I_{\mathrm{m}}^{i}, \mathbf{x}\right)$ is instead given from Equation (12) as:

$$I_{e}^{i}\left(V_{\mathrm{m}}^{i}, I_{\mathrm{m}}^{i}, \mathbf{x}\right) = I_{\mathrm{L}} - I_{01}\left[\exp\left(\frac{q\left(V_{\mathrm{m}}^{i} + R_{\mathrm{s}} \cdot I_{\mathrm{m}}^{i}\right)}{n_{1} \cdot k \cdot T_{c}}\right) - 1\right] - I_{02}\left[\exp\left(\frac{q\left(V_{\mathrm{m}}^{i} + R_{\mathrm{s}} \cdot I_{\mathrm{m}}^{i}\right)}{n_{2} \cdot k \cdot T_{c}}\right) - 1\right] - \frac{V_{\mathrm{m}}^{i} + R_{\mathrm{s}} \cdot I_{\mathrm{m}}^{i}}{R_{\mathrm{p}}} \tag{30}$$

where $\mathbf{x} = \left[R_{\mathrm{s}}, R_{\mathrm{p}}, I_{\mathrm{L}}, I_{01}, I_{02}, n_{1}, n_{2}\right]$ denotes the set of decision variables (seven) related to the DD model of a solar cell [5]. As suggested by Equation (28), the proposed objective function is formulated by using experimental data corresponding to a series of I-V measurements, extracted from a real solar cell. Such experimental data could also be acquired from PV cell datasheets, which are usually provided by cell manufacturers. It is important to consider that, as a result of several issues related to the data collection process, the extracted measurements are usually subject to contain noise. These fact causes the objective function to present several other challenging characteristics, such as high-multimodality and the presence of noisy features [2,10,11].

5. Experimental Setup and Results

In this paper, the CGSA optimization method [24] is proposed to solve the problem of accurate electrical parameters estimation in PV cells. For our experiments, we considered the set of PV cell I-V measurements illustrated in [30]. Such set of measurements were extracted from a commercial 57 mm diameter silicon PV cell (manufactured by the R.T.C. Company, Paris, Île-de-France, France), while being tested under certain specific conditions (specifically, solar intensity $G = 1000\ \mathrm{W/m^2}$ and cell temperature $T_c = 33\ ^\circ\mathrm{C}$). Such a set of I-V measurements was chosen in order to establish a better comparison with other previously published works ([1,2,12,31]). Furthermore, we also considered two additional sets of I-V measurements, extracted from two other state-of-the art PV devices for our experiments: (1) a KC200GT PV module (Kyocera Solar Inc., Scottsdale, AZ, USA) and (2) a SM55 Solar Panel (Siemens Solar Industries, Camarillo, CA, USA). For each of our experiments, the root mean squared error (RMSE) between a set of measured I-V characteristics (this is, the current and voltages measurements provided by the real PV cell under particular test conditions) and a set of experimental data (comprised by the calculated current and voltage characteristics with regard to either the SD or DD model) is considered to evaluate resemblance between the PV cell's real I-V characteristics and those provided by our proposed estimation approach. In this section, we included two different sets of experimental results: First, in Section 5.1 we show simulation results corresponding to the implementation of our proposed CGSA-based solar cell parameter identification approach, in which, we study the effects of incorporating several different types of chaotic map functions into the gravitational constant of CGSA. Finally, in Section 5.2, a series of comparative experiments against other similar PV cell parameter extraction methods are presented.

5.1. CGSA-Based Implementation for PV Cells Parameter Estimation

As illustrated in Section 3, the CGSA [24] is a modified version to the original GSA proposed in [19] in which, a particular chaotic map function $C(t)$ is added to the gravitational constant $G(t)$ in order to "chaotically" modify its intensity at each iteration t, which further aids to balance the exploration and exploitation properties of search agents. In the context of our proposed CGSA-based approach, the electrical parameters of a solar cell (decision variables) are encoded as agent positions $\mathbf{x} = [x_1, x_2, \ldots, x_d]$ within a d-dimensional system of masses. As illustrated in Section 4, the representation of such set of decision variables is dependent on the particular circuit model used to describe the behavior of the PV cell (either SD model or DD model). In our proposed approach, the mass of each search agent is calculated by considering the RMSE between the PV cell's measured I-V characteristics and those estimated by considering a particular solar cell model (see Section 4) [2]. With that being said, the PV cell parameter estimation problem may be more formally expressed as:

$$
\begin{array}{lcc}
\text{minimize} & \multicolumn{2}{c}{\mathrm{RMSE}(\mathbf{X}),\ \mathbf{X} = \left[\mathbf{x}_1, \mathbf{x}_2, \ldots, \mathbf{x}_{N_p}\right],\ \mathbf{x}_i = [x_{i,1}, x_{i,2}, \ldots, x_{i,d}]\ d \in [5,7]} \\
 & \text{for the single diode (SD) model} & \text{for the double diode (SD) model} \\
 & d = 5 & d = 7 \\
 & 0 \le x_{i,1}(R_\mathrm{s}) \le 0.5 & 0 \le x_{i,1}(R_\mathrm{s}) \le 0.5 \\
 & 0 \le x_{i,2}(R_\mathrm{p}) \le 100 & 0 \le x_{i,2}(R_\mathrm{p}) \le 100 \\
\text{subject to :} & 0 \le x_{i,3}(I_\mathrm{L}) \le 1 & 0 \le x_{i,3}(I_\mathrm{L}) \le 1 \\
 & 0 \le x_{i,4}(I_0) \le 1 & 0 \le x_{i,4}(I_{01}) \le 1 \\
 & 0 \le x_{i,5}(n) \le 2 & 0 \le x_{i,5}(I_{02}) \le 1 \\
 & & 0 \le x_{i,6}(n_1) \le 2 \\
 & & 0 \le x_{i,7}(n_2) \le 2
\end{array}
\tag{31}
$$

where N_p stand for the number of available search agents (population size), while d denotes the total number of decision variables (dimensions). Similarly to the experiments reported in [24], we evaluated the performance of the proposed CGSA-based approach with regard to 10 different chaotic map functions. For all cases, the initial gravitational constant value of CGSA is set to $G_0 = 100$, while the constant parameter alpha is set to $\alpha = 20$ (see Equation (25)). Also, the minimum and maximum values for the chaotic function's adaptive interval are set to $min = 1 \times 10^{-10}$ and $max = 17.0$, respectively (see Equation (27)). A detailed list of all chaotic functions applied in our experiments may be found in Appendix A. In Table 1, the minimization results averaged over 30 individual runs (each considering $t = 4000$ iterations and $N_p = 100$ search agents) for both the SD a DD models, obtained by CGSA with regard to each of the proposed chaotic map function (1 through 10), are shown. The reported results consider three particular performance indexes: The average best RMSE (AB_{RMSE}), the median best RMSE (MB_{RMSE}) and the standard deviation of the RMSE values (STD_{RMSE}). Note that the best outcomes for each of the simulated solar cell models are boldfaced. As evidenced by these results, overall, CGSA-6 ranks the best from among all of the tested chaos-embedded GSA approaches, and as such, it is specifically considered for the rest of our experiments.

Table 1. CGSA minimization results for the SD and DD models (with $G = 1000\ \mathrm{W/m^2}$ and $T_c = 33\ ^\circ\mathrm{C}$), for 30 individual runs (with $t = 4000$ iterations each and $N_p = 100$ search agents). Note that the best outcomes for each of the simulated solar cell models are boldfaced.

Method	Embedded Chaotic Map ($C_i(t)$)	Single-Diode (SD) Model			Double-Diode (DD) Model		
		AB_{RMSE}	MB_{RMSE}	STD_{RMSE}	AB_{RMSE}	MB_{RMSE}	STD_{RMSE}
CGSA-1	$C_1(t)$ (Chebyshev)	4.38×10^{-2}	3.41×10^{-2}	5.58×10^{-4}	12.7×10^{-1}	10.3×10^{-1}	4.99×10^{-7}
CGSA-2	$C_2(t)$ (Circle)	2.77×10^{-2}	1.60×10^{-2}	6.69×10^{-4}	40.6×10^{-1}	52.4×10^{-1}	6.81×10^{-7}
CGSA-3	$C_3(t)$ (Gauss/Mouse)	1.34×10^{-1}	3.38×10^{-1}	1.23×10^{-3}	53.9×10^{-1}	53.9×10^{-1}	4.12×10^{-7}
CGSA-4	$C_4(t)$ (Iterative)	7.31×10^{-2}	8.98×10^{-2}	6.27×10^{-4}	39.6×10^{-1}	41.7×10^{-1}	5.23×10^{-7}
CGSA-5	$C_5(t)$ (Logistic)	1.34×10^{-1}	1.24×10^{-1}	5.94×10^{-4}	92.6×10^{-1}	87.9×10^{-1}	1.68×10^{-7}
CGSA-6	$C_6(t)$ (Piecewise)	$\mathbf{7.05 \times 10^{-3}}$	$\mathbf{7.32 \times 10^{-3}}$	6.10×10^{-4}	$\mathbf{3.22 \times 10^{-4}}$	$\mathbf{2.63 \times 10^{-4}}$	$\mathbf{1.63 \times 10^{-7}}$
CGSA-7	$C_7(t)$ (Sine)	5.14×10^{-2}	4.39×10^{-2}	7.16×10^{-4}	84.3×10^{-1}	70.7×10^{-1}	2.53×10^{-8}
CGSA-8	$C_8(t)$ (Singer)	7.05×10^{-2}	3.73×10^{-2}	$\mathbf{4.74 \times 10^{-4}}$	7.28×10^{-1}	6.15×10^{-1}	9.39×10^{-7}
CGSA-9	$C_9(t)$ (Sinusoidal)	1.98×10^{-2}	3.58×10^{-2}	6.52×10^{-4}	55.4×10^{-1}	60.4×10^{-1}	1.85×10^{-6}
CGSA-10	$C_{10}(t)$ (Tent)	2.56×10^{-2}	4.56×10^{-2}	6.20×10^{-4}	18.5×10^{-1}	27.5×10^{-1}	2.77×10^{-6}

Furthermore, in Table 2, the CGSA-6 absolute and relative error values ($\varepsilon_{\mathrm{abs}}$ and ε_{r}, respectively), corresponding to the comparison between the measured and experimental I-V data for both the SD and DD models, are shown. This pair of error measurements are given by the following equations:

$$\varepsilon_{\mathrm{abs}} = |I_{\mathrm{m}} - I_{\mathrm{e}}| \tag{32}$$

$$\varepsilon_{\mathrm{r}} = \left| \frac{I_{\mathrm{m}} - I_{\mathrm{e}}}{I_{\mathrm{m}}} \right| \cdot 100 \tag{33}$$

where I_{m} and I_{e} stand for the measured and calculated PV cell's current, respectively. Note that for both models, the RMSE between both the measured and estimated I-V data is presented.

Also, in Table 3, the best set of electrical PV cell parameters, extracted by applying the CGSA-6 for both the SD and DD models, are presented. Also, in Figure 5, we show the comparison between the measured and estimated I-V characteristic curves for both the SD and DD models. As observed in such figure, the estimated I-V curves provide a very close approximation to those produced by the provided experimental measurements.

In addition to the previously illustrated experiments, we also implemented our proposed approach to estimate the electrical parameters of two other PV devices, namely a Kyocera KC200GT PV module (composed of 54 individual PV cells) and a Siemens SM55 Solar Panel (composed of 36 individual PV cells). For our experiments, we considered the I-V characteristics of individual PV cells rather than those of the complete PV module. Furthermore, such PV cells I-V measurements were extracted by considering several different test conditions, namely, solar irradiance levels (G) of 200, 400, 600, 800 and 1000 $\mathrm{W/m^2}$ and a fixed cell temperature (T_c) of 33 °C. For each case, we applied our proposed CGSA-6 based approach to estimate the PV cell parameters corresponding to both the SD and DD models. In Table 4, the RMSE values between the measured and experimental I-V characteristics for a single solar cell of the aforementioned PV modules (Kyocera KC200GT and Siemens SM55), at each of the considered solar irradiance conditions are shown. Furthermore, Figures 6 and 7 show the measured and estimated (experimental) I-V curves for both of the considered PV cells at each different test condition. From these figures it could be appreciated that our proposed PV cell parameters estimation approach produce close approximations to the real I-V characteristics of each implemented PV cell, independently of the considered solar irradiance conditions. In addition, Tables 5 and 6 show the PV cell parameter combinations extracted for both of the considered PV cells with regard to the SD and DD models respectively.

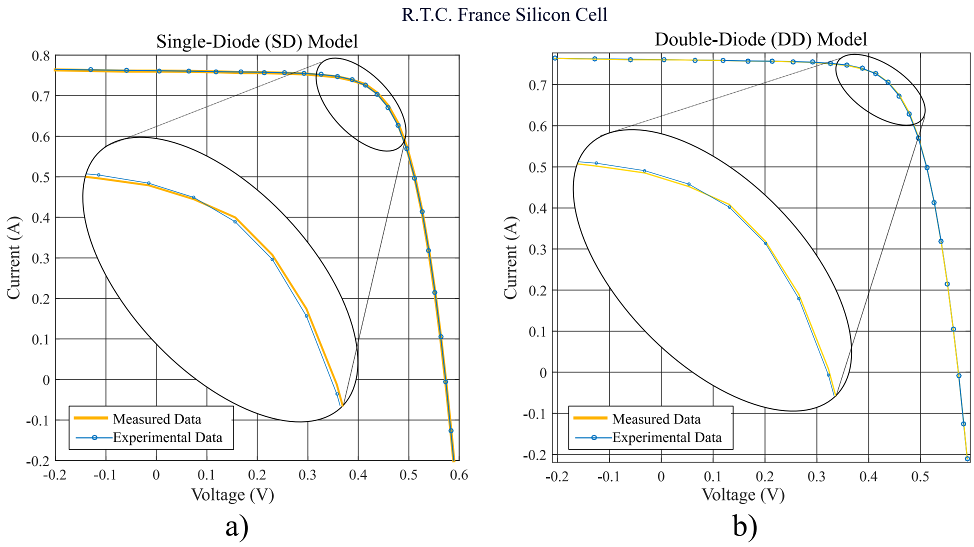

Figure 5. PV Cell's measured and estimated I-V characteristics for (**a**) SD model and (**b**) DD model under specific test conditions ($G = 1000\ \mathrm{W/m^2}$ and $T_c = 33$ °C).

Table 2. CGSA-6 absolute and relative error values for the SD and DD models with regard to the extracted PV cell I-V measurements at specific test conditions ($G = 1000\ \mathrm{W/m^2}$ and $T_c = 33\ ^\circ\mathrm{C}$).

Measurements	Measured Voltage V_m (V)	Measured Current I_m (A)	Single-Diode (SD) Model			Double-Diode (DD) Model		
			Estimated Current I_e (A)	Absolute Error $''_{abs}$	Relative Error $''_r$ (%)	Estimated Current I_c (A)	Absolute Error $''_{abs}$	Relative Error $''_r$ (%)
1	−0.2057	0.7640	0.7643	2.8067×10^{-4}	0.0367	0.7651	1.0669×10^{-3}	0.1029
2	−0.1291	0.7620	0.7630	1.0210×10^{-3}	0.1340	0.7639	1.7823×10^{-3}	0.0998
3	−0.0588	0.7605	0.7619	1.3646×10^{-3}	0.1794	0.7626	2.1029×10^{-3}	0.0969
4	0.0057	0.7605	0.7608	3.0200×10^{-4}	0.0397	0.7615	1.0189×10^{-3}	0.0942
5	0.0646	0.7600	0.7598	1.7127×10^{-4}	0.0225	0.7605	5.2526×10^{-4}	0.0917
6	0.1185	0.7590	0.7589	7.2747×10^{-5}	0.0096	0.7596	6.0257×10^{-4}	0.0890
7	0.1678	0.7570	0.7581	1.0693×10^{-3}	0.1412	0.7587	1.7186×10^{-3}	0.0857
8	0.2132	0.7570	0.7572	1.8295×10^{-4}	0.0242	0.7578	7.9334×10^{-4}	0.0806
9	0.2545	0.7555	0.7561	6.4155×10^{-4}	0.0849	0.7567	1.1865×10^{-3}	0.0720
10	0.2924	0.7540	0.7546	6.4702×10^{-4}	0.0858	0.7551	1.0781×10^{-3}	0.0571
11	0.3269	0.7505	0.7522	1.6731×10^{-3}	0.2229	0.7524	1.9165×10^{-3}	0.0324
12	0.3585	0.7465	0.7478	1.2585×10^{-3}	0.1686	0.7477	1.2147×10^{-3}	0.0059
13	0.3873	0.7385	0.7399	1.4468×10^{-3}	0.1959	0.7395	1.0101×10^{-3}	0.0590
14	0.4137	0.7280	0.7265	1.5279×10^{-3}	0.2099	0.7256	2.4359×10^{-3}	0.1250
15	0.4373	0.7065	0.7053	1.2021×10^{-3}	0.1702	0.7039	2.5711×10^{-3}	0.1941
16	0.459	0.6755	0.6730	2.4956×10^{-3}	0.3694	0.6713	4.2027×10^{-3}	0.2537
17	0.4784	0.6320	0.6283	3.7150×10^{-3}	0.5878	0.6265	5.5017×10^{-3}	0.2844
18	0.496	0.5730	0.5698	3.2231×10^{-3}	0.5625	0.5682	4.7716×10^{-3}	0.2718
19	0.5119	0.4990	0.4982	7.5105×10^{-4}	0.1505	0.4972	1.7792×10^{-3}	0.2063
20	0.5265	0.4130	0.4134	4.3597×10^{-4}	0.1056	0.4131	1.3916×10^{-4}	0.0718
21	0.5398	0.3165	0.3184	1.9494×10^{-3}	0.6159	0.3189	2.3934×10^{-3}	0.1394
22	0.5521	0.2120	0.2140	1.9730×10^{-3}	0.9307	0.2150	3.0083×10^{-3}	0.4838
23	0.5633	0.1035	0.1043	8.3512×10^{-4}	0.8069	0.1056	2.1143×10^{-3}	1.2260
24	0.5736	−0.0100	−0.0074	2.5833×10^{-3}	25.8330	-0.0065	3.5048×10^{-3}	12.4252
25	0.5833	−0.1230	−0.1258	2.7619×10^{-3}	2.2455	-0.1256	2.6384×10^{-3}	0.0983
26	0.59	−0.2100	−0.2110	9.5888×10^{-4}	0.4566	-0.2120	2.0566×10^{-3}	0.5204
	RMSE (Measured VS Estimated Data)			4.6897×10^{-5}			3.0179×10^{-5}	

Table 3. PV cell parameters for the SD and DD models, extracted by applying the proposed CGSA-6 approach.

Single-Diode (SD) Model		Double-Diode (DD) Model	
Parameter	**Value**	**Parameter**	**Value**
R_s (Ω)	0.0319	R_s (Ω)	0.0336
R_p (Ω)	59.5804	R_p (Ω)	60.8
I_L (A)	0.7620	I_L (A)	0.0761
I_0 (μA)	8.45×10^{-7}	I_{01} (μA)	2.13×10^{-9}
n	1.5858	I_{02} (μA)	5.93×10^{-7}
-	-	n_1	1.8871
-	-	n_2	1.5458

Table 4. RMSE values between the measured and estimated I-V characteristics at different solar irradiance levels (200, 400, 600, 800 and 1000 W/m^2) and fixed cell temperature (T_c = 33 °C), extracted from an individual PV cell from both the Kyocera KC200GT and Siemens SM55 Solar Panels.

Solar Irradiance G (W/m^2)	Kyocera KC200GT (T_c = 33 °C)		Siemens SM55 (T_c = 33 °C)	
	Single-Diode (SD) Model	Double-Diode (DD) Model	Single-Diode (SD) Model	Double-Diode (DD) Model
200	8.6164×10^{-4}	9.1310×10^{-4}	3.8232×10^{-4}	3.7282×10^{-4}
400	2.5204×10^{-3}	2.5440×10^{-3}	1.8303×10^{-4}	1.2043×10^{-4}
600	3.1025×10^{-3}	2.0321×10^{-3}	2.3460×10^{-4}	4.0115×10^{-4}
800	4.4104×10^{-3}	4.7491×10^{-3}	4.5745×10^{-4}	9.1752×10^{-4}
1000	4.8793×10^{-3}	4.8801×10^{-3}	4.5589×10^{-4}	1.0381×10^{-3}

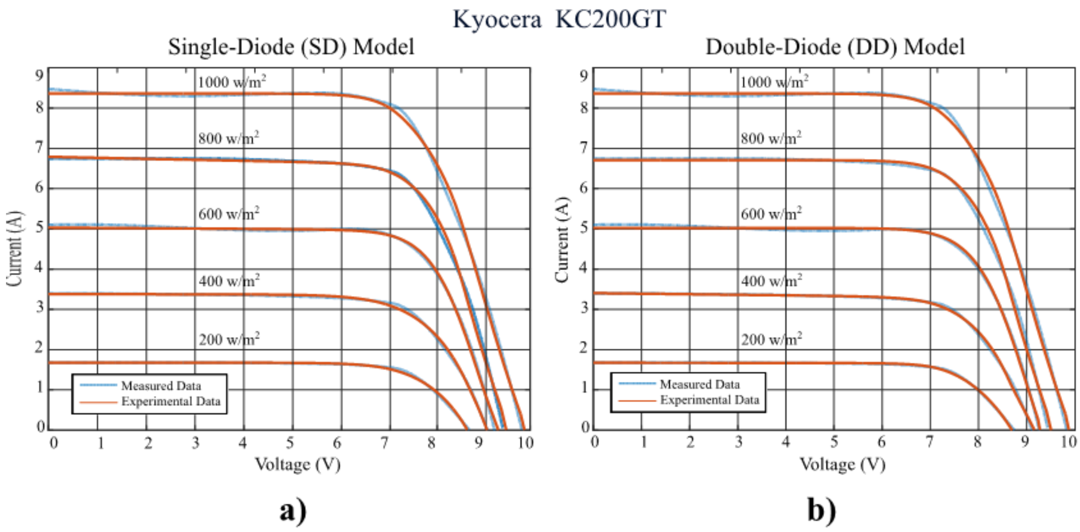

Figure 6. Estimated I-V characteristics curves at different irradiance levels (200, 400, 600, 800 and 1000 W/m^2) and fixed cell temperature (T_c = 33 °C) for an individual cell from a Kyocera KC200GT Solar Panel. (**a**) SD model and (**b**) DD model.

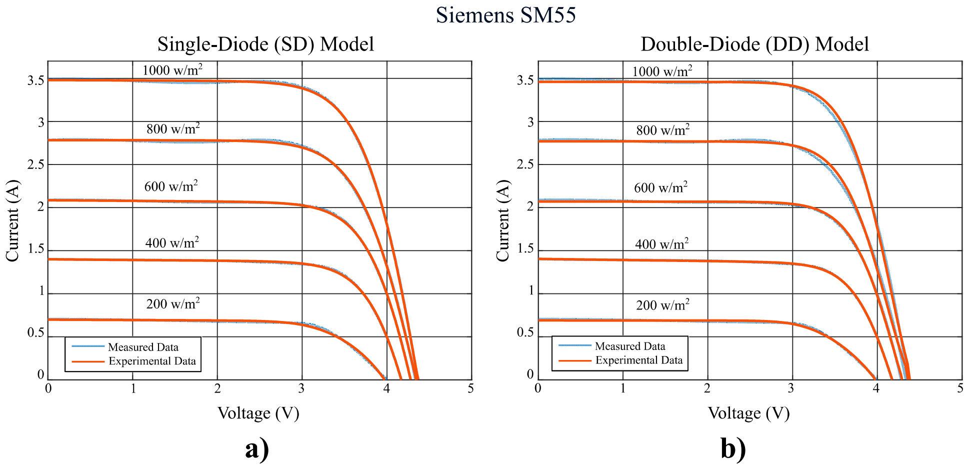

Figure 7. Estimated I-V characteristics curves at different irradiance levels (200, 400, 600, 800 and 1000 W/m^2) and fixed cell temperature ($T_c = 33$ °C) for an individual cell from a Siemens SM55 Solar Panel. (**a**) SD model and (**b**) DD model.

Table 5. SD model PV cell parameters at different solar irradiance levels (200, 400, 600, 800 and 1000 W/m^2) and fixed cell temperature ($T_c = 33$ °C), extracted by considering an individual PV cell from both the Kyocera KC200GT and Siemens SM55 Solar Panels.

Single-Diode (SD) Model ($T_c = 33$ °C)					
Kyocera KC200GT					
Solar Irradiance G (W/m^2)	**R_s (Ω)**	**R_p (Ω)**	**I_L (A)**	**I_0 (μA)**	**n**
200	4.2433 $\times 10^{-2}$	158.4481	1.6715	1.1715 $\times 10^{-9}$	1.8813
400	2.6891 $\times 10^{-2}$	6.1693	3.4373	1.9518 $\times 10^{-9}$	1.9533
600	1.5950 $\times 10^{-2}$	414.4098	5.0228	3.5778 $\times 10^{-9}$	2.0
800	1.6710 $\times 10^{-2}$	4.8187	6.8122	1.1162 $\times 10^{-9}$	1.9111
100	1.9828 $\times 10^{-2}$	477.4431	8.3612	1.6264 $\times 10^{-9}$	2.0
Siemens SM55					
Solar Irradiance G (W/m^2)	**R_s (Ω)**	**R_p (Ω)**	**I_L (A)**	**I_0 (μA)**	**n**
200	8.3263 $\times 10^{-2}$	38.2415	0.7001	6.5351 $\times 10^{-8}$	1.6005
400	1.8277 $\times 10^{-2}$	21.1100	1.4006	1.4490 $\times 10^{-7}$	1.6851
600	1.7189 $\times 10^{-2}$	24.7559	2.0857	2.6572 $\times 10^{-7}$	1.7511
800	1.9223 $\times 10^{-2}$	499.6838	2.7819	1.0671 $\times 10^{-6}$	1.9067
100	1.3889 $\times 10^{-2}$	44.9859	3.4807	1.0461 $\times 10^{-6}$	1.8861

Table 6. DD model PV cell parameters at different solar irradiance levels (200, 400, 600, 800 and 1000 W/m^2) and fixed cell temperature ($T_c = 33$ °C), extracted by considering an individual PV cell from both the Kyocera KC200GT and Siemens SM55 Solar Panels.

Double-Diode (DD) Model ($T_c = 33$ °C)							
Kyocera KC200GT							
Solar Irradiance G (W/m^2)	**R_s (Ω)**	**R_p (Ω)**	**I_L (A)**	**I_{01} (μA)**	**I_{02} (μA)**	**n_1**	**n_2**
200	4.5609 $\times 10^{-2}$	230.8024	1.6709	2.9690 $\times 10^{-10}$	9.8390 $\times 10^{-15}$	1.7665	1.8685
400	2.7970 $\times 10^{-2}$	285.2671	3.3561	3.2445 $\times 10^{-9}$	4.4788 $\times 10^{-16}$	2.0	1.7147
600	1.5041 $\times 10^{-2}$	5.1980	5.1186	3.5308 $\times 10^{-9}$	9.9806 $\times 10^{-12}$	2.0	1.9809
800	1.6433 $\times 10^{-2}$	161.0079	6.7092	3.0386 $\times 10^{-9}$	6.0391 $\times 10^{-11}$	2.0	1.9955
100	1.9833 $\times 10^{-2}$	388.8951	8.3616	2.6188 $\times 10^{-9}$	1.6193 $\times 10^{-9}$	1.9215	2.0
Siemens SM55							
Solar Irradiance G (W/m^2)	**R_s (Ω)**	**R_p (Ω)**	**I_L (A)**	**I_{01} (μA)**	**I_{02} (μA)**	**n_1**	**n_2**
200	0.1029	499.4715	0.6900	2.69203 $\times 10^{-9}$	4.55723 $\times 10^{-12}$	1.3379	1.7990
400	2.56063 $\times 10^{-2}$	13.2527	1.4065	9.42853 $\times 10^{-9}$	1.81753 $\times 10^{-9}$	1.4421	1.9917
600	2.35263 $\times 10^{-2}$	297.4967	2.0699	8.06543 $\times 10^{-9}$	9.93913 $\times 10^{-9}$	1.4736	1.5282
800	2.65863 $\times 10^{-2}$	186.3662	2.7700	3.60713 $\times 10^{-11}$	9.99453 $\times 10^{-9}$	1.3452	1.4530
100	1.95903 $\times 10^{-2}$	415.5791	3.4597	2.51183 $\times 10^{-9}$	9.99713 $\times 10^{-9}$	1.4258	1.4714

Finally, in Figures 8 and 9 we show curves corresponding to the absolute error between the measured and experimental I-V data for both of the considered PV cells at each of the different solar intensity conditions. From such curves we can observe that in general the absolute error between the measured and experimental data increases as the solar intensity increases. In a similar manner to the previously reported experiments, we also tested our proposed PV cell parameter extraction scheme for the case of different cell temperature conditions (T_c) and a fixed solar intensity (G). In particular, we have done experiments by considering cell temperatures of 25, 50 and 75 °C and a solar irradiance of 1000 W/m^2. As illustrated in [32], the performance of a PV cell is notably sensitive to the cell's operating temperature. In particular, as the operating temperature T_c of a PV cell increases, its overall performance decays. This phenomenon is more notably noticed as a decrease on the PV cell's photocurrent, which conversely yields to a decrease on the overall cell's output voltage.

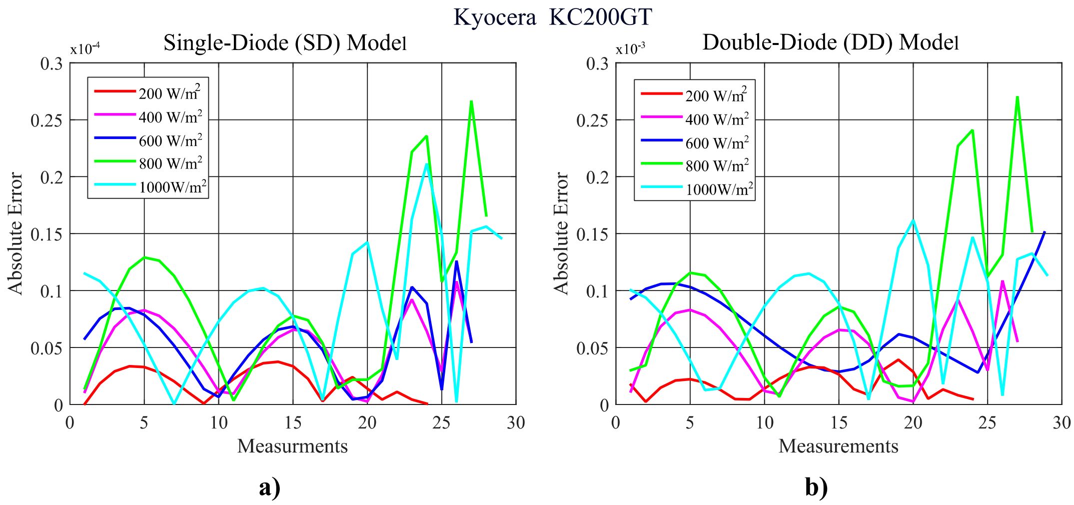

Figure 8. Absolute error curves between the measured and experimental I-V data at different irradiance levels (200, 400, 600, 800 and 1000 W/m^2) and fixed cell temperature ($T_c = 33$ °C) for an individual cell from a Kyocera KC200GT Solar Panel. (**a**) SD model and (**b**) DD model.

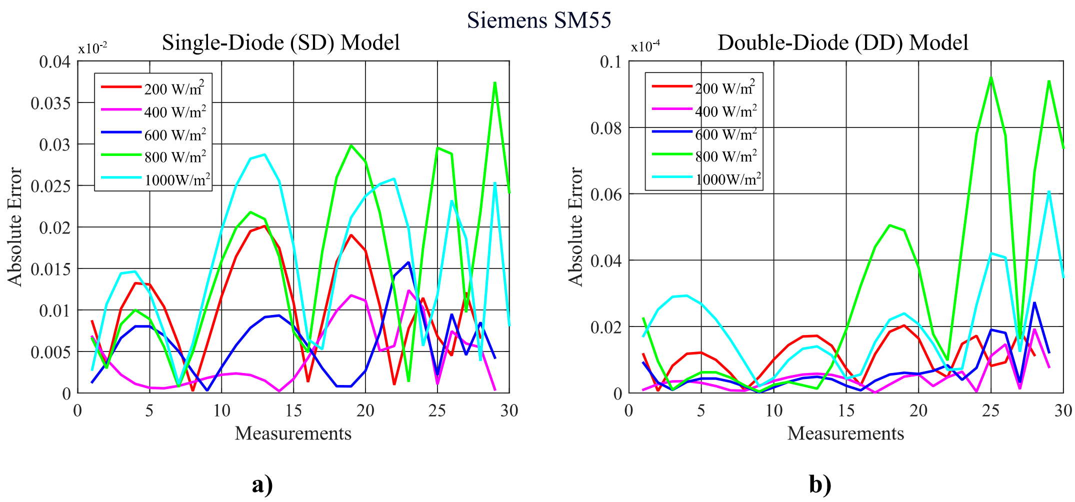

Figure 9. Absolute error curves between the measured and experimental I-V data at different irradiance levels (200, 400, 600, 800 and 1000 W/m^2) and fixed cell temperature ($T_c = 33$ °C) for an individual cell from a Siemens SM55 Solar Panel. (**a**) SD model and (**b**) DD model.

In Table 7, we show the RMSE values corresponding to the comparison between the measured and experimental I-V characteristics for each of the considered PV cells and cell temperature conditions, and with regard to both the SD and DD PV cell models. Furthermore, the measured and experimental I-V curves for each of the considered cell temperatures and PV cell models (SD and DD) are shown in Figures 10 and 11. Similarly to Figures 6 and 7, it could be appreciated that the proposed CGSA-6 based PV cell parameter estimation approach produce a close approximation to the real PV cell I-V characteristics at each of the considered cell temperature conditions. Also, Tables 8 and 9 show the PV cell parameter combinations extracted for both of the tested PV cells, with regard to the SD and DD models respectively. Finally, Figures 12 and 13 show curves corresponding to the absolute error between the measured and experimental I-V data for both of the considered PV cells at each different cell temperature conditions. Similarly to the case of varying solar irradiance levels, it could be observed that the value of the absolute differences between the measured and experimental data tends to increases as the cell temperature increases.

Table 7. RMSE values between the measured and estimated I-V characteristics at different cell temperatures (25, 50 and 75 °C) and fixed solar irradiance (G = 1000 W/m^2), extracted from an individual PV cell from both the Kyocera KC200GT and Siemens SM55 Solar Panels.

Cell Temperature T_c (°C)	**Kyocera KC200GT (G = 1000 W/m^2)**		**Siemens SM55 (G = 1000 W/m^2)**	
	Single-Diode (SD) Model	**Double-Diode (DD) Model**	**Single-Diode (SD) Model**	**Double-Diode (DD) Model**
25	4.8793×10^{-3}	4.8801×10^{-3}	4.5490×10^{-4}	9.7603×10^{-4}
50	3.1599×10^{-3}	3.1626×10^{-3}	8.7597×10^{-4}	1.3058×10^{-3}
75	5.7532×10^{-3}	1.0944×10^{-2}	1.6080×10^{-3}	1.1646×10^{-3}

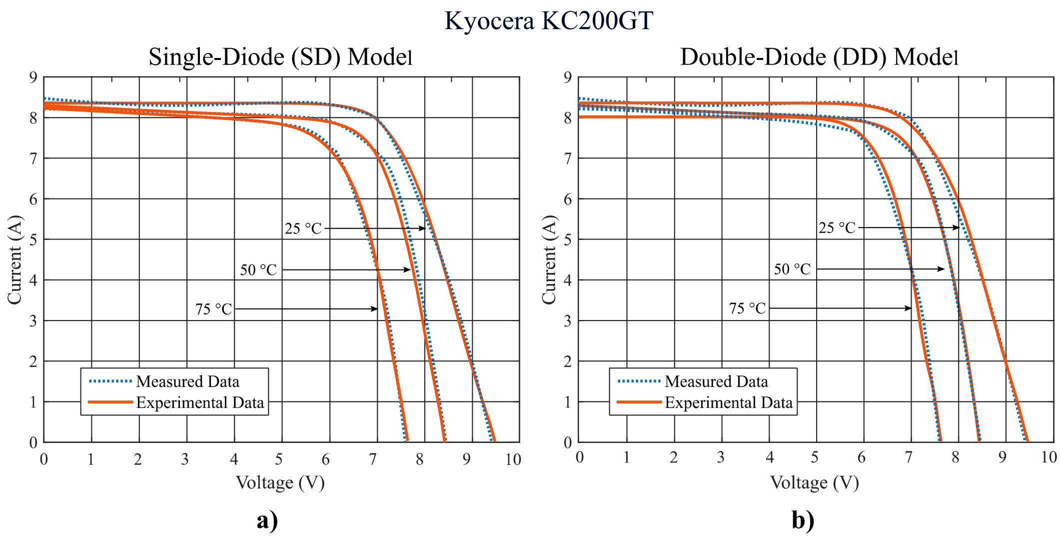

Figure 10. Estimated I-V characteristics curves at different cell temperatures (25, 50 and 75 °C) and fixed solar irradiance (G = 1000 W/m^2) for an individual cell from a Kyocera KC200GT Solar Panel. (**a**) SD model and (**b**) DD model.

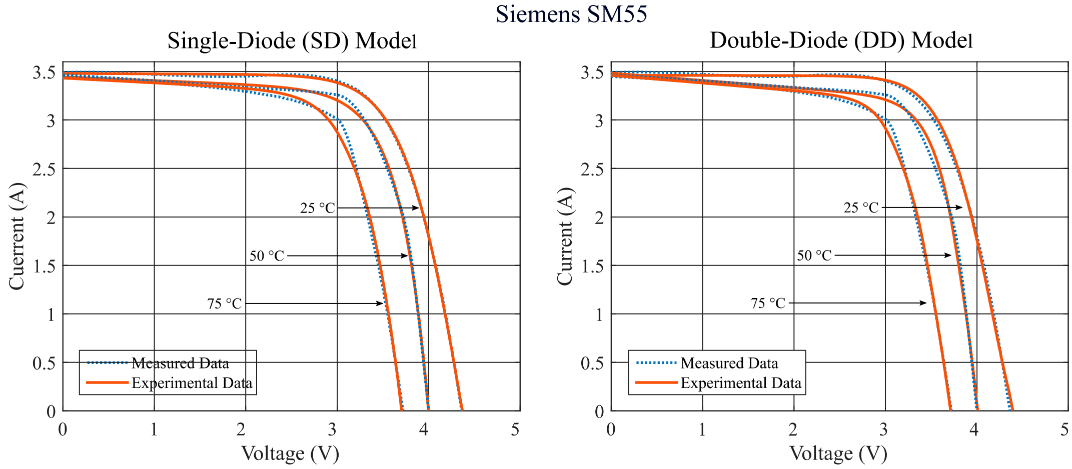

Figure 11. Estimated I-V characteristics curves at different cell temperatures (25, 50 and 75 °C) and fixed solar irradiance ($G = 1000\ \mathrm{W/m^2}$) for an individual cell from a Kyocera KC200GT Solar Panel. (**a**) SD model and (**b**) DD model.

Table 8. SD model PV cell parameters at different cell temperatures (25, 50 and 75 °C) and fixed solar irradiance ($G = 1000\ \mathrm{W/m^2}$), extracted by considering an individual PV cell from both the Kyocera KC200GT and Siemens SM55 Solar Panels.

Single-Diode (SD) Model ($G = 1000$ W/m^2)					
Kyocera KC200GT					
Cell Temperature T_c (°C)	**R_s (Ω)**	**R_p (Ω)**	**I_L (A)**	**I_0 (μA)**	**n**
25	1.9828×10^{-2}	477.4431	8.3612	1.6264×10^{-9}	2.0
50	7.9339×10^{-3}	2.1511	8.3255	5.1797×10^{-9}	1.8146
75	7.1330×10^{-3}	1.7953	8.2661	2.3448×10^{-7}	1.9999
Siemens SM55					
Cell Temperature T_c (°C)	**R_s (Ω)**	**R_p (Ω)**	**I_L (A)**	**I_0 (μA)**	**n**
25	1.4107×10^{-2}	37.8178	3.4814	8.9007×10^{-7}	1.8662
50	5.4227×10^{-8}	4.4091	3.4442	7.4646×10^{-6}	1.9964
75	9.8848×10^{-3}	3.3479	3.4424	1.7497×10^{-6}	1.6678

Table 9. DD model PV cell parameters at different cell temperatures (25, 50 and 75 °C) and fixed solar irradiance ($G = 1000\ \mathrm{W/m^2}$), extracted by considering an individual PV cell from both the Kyocera KC200GT and Siemens SM55 Solar Panels.

Double-Diode (DD) Model ($G = 1000$ W/m^2)							
Kyocera KC200GT							
Cell Temperature T_c (°C)	**R_s (Ω)**	**R_p (Ω)**	**I_L (A)**	**I_{01} (μA)**	**I_{02} (μA)**	**n_1**	**n_2**
25	1.9833×10^{-2}	388.8951	8.3616	2.6188×10^{-12}	1.6193×10^{-9}	1.9215	2.0
50	7.8702×10^{-3}	2.1365	8.3272	2.6724×10^{-9}	3.4995×10^{-9}	1.8760	1.8066
75	9.4247×10^{-3}	476.3930	8.0211	1.5302×10^{-9}	9.9997×10^{-9}	1.6951	1.7047
Siemens SM55							
Cell Temperature T_c (°C)	**R_s (Ω)**	**R_p (Ω)**	**I_L (A)**	**I_{01} (μA)**	**I_{02} (μA)**	**n_1**	**n_2**
25	1.9279×10^{-2}	139.7075	3.4613	9.9180×10^{-9}	6.5290×10^{-9}	1.4783	1.4832
50	7.7897×10^{-3}	2.2004	3.4952	9.9996×10^{-9}	8.0770×10^{-9}	1.7329	1.3135
75	1.6458×10^{-2}	2.1069	3.4868	3.7651E $\times 10^{-9}$	3.8184×10^{-9}	1.1735	1.6896

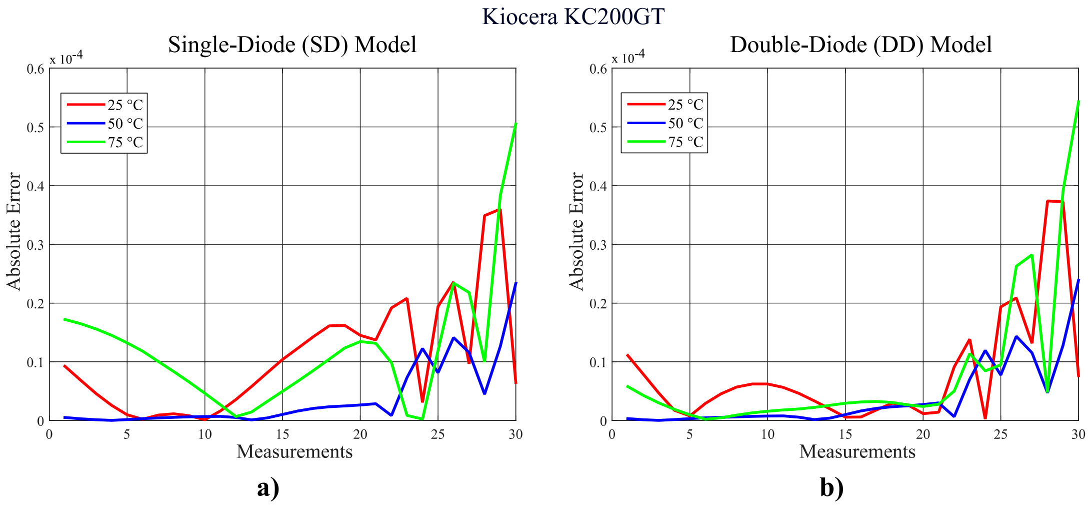

Figure 12. Absolute error curves between the measured and experimental I-V data at different cell temperatures (25, 50 and 75 °C) and fixed solar irradiance ($G = 1000\ \mathrm{W/m^2}$) for an individual cell from a Kyocera KC200GT Solar Panel. (**a**) SD model and (**b**) DD model.

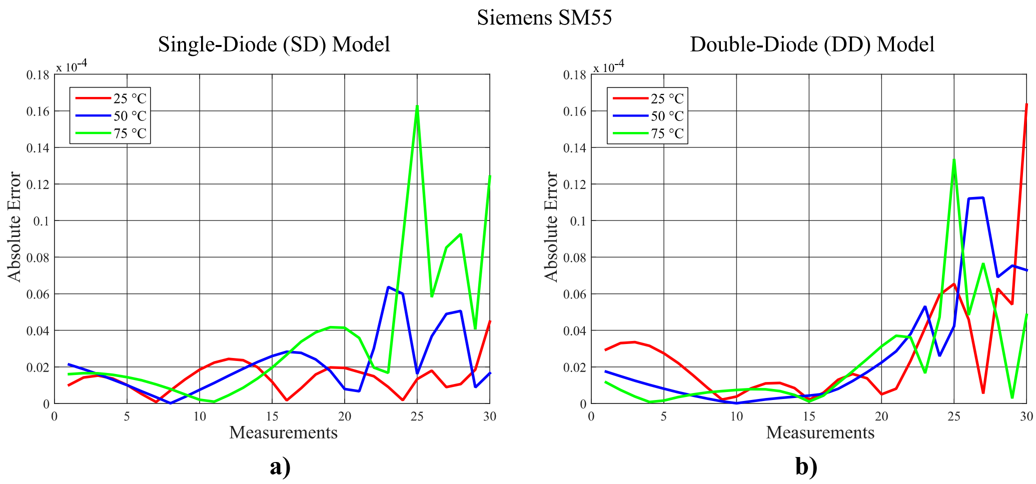

Figure 13. Absolute error curves between the measured and experimental I-V data at different cell temperatures (25, 50 and 75 °C) and fixed solar irradiance ($G = 1000\ \mathrm{W/m^2}$) for an individual cell from a Siemens SM55 Solar Panel. (**a**) SD model and (**b**) DD model.

5.2. Comparison with Other Intelligent PV Cell Parameter Estimation Approaches

In Section 5.1, we compared the performance of our proposed CGSA-based PV cell parameter estimation method with regard to several different embedded chaotic map functions. From these comparisons we concluded that, for the proposed PV cell parameter estimation problem, the CGSA-6 approach ranks the best from among all of the tested CGSA variants.

In order to further demonstrate the proficiency of the CGSA-6 approach for solving the problem of accurate PV cell parameters identification, a series of comparative experiments against other similar implementations, currently reported on the literature, were performed. For our comparisons, we considered other well-known intelligent optimization approaches such as the original Gravitational Search Algorithm (GSA) [19], the Particle Swarm Optimization (PSO) method [13], the Harmony Search (HS) strategy [33], the Firefly Algorithm (FA) [34], and the Differential Evolution (DE) approach [16]. The chosen parameter settings for each implemented algorithm is described as follows:

1. GSA: The initial value for the gravitation constant is set to $G_o = 100$, while the constant parameter alpha is set as $\alpha = 20$ [19].
2. PSO: The cognitive and social coefficients are set to $c_1 = 2.0$ and $c_2 = 2.0$, respectively. Also, the inertia weight factor ω is set to decreases linearly from 0.9 to 0.2 as the search process evolves [13].
3. HA: The values for distance bandwidth, harmony memory considering rate and pitch adjustment ratio are set to $d = 0.2$, $h = 0.95$, and $p = 0.3$, respectively [33].
4. FA: The randomness factor and light absorption coefficient are set to $\alpha = 0.2$ and $\gamma = 1.0$, respectively [34].
5. DE: The algorithm's differential weight and crossover probability are set to $w = 1$ and $c = 0.2$, respectively [16].
6. CGSA-6: The parameter setup for this method is as illustrated in Section 5.1 ($G_o = 100$, $\alpha = 20$, $min = 1 \times 10^{-10}$, $max = 17.0$ and $C_i(t) = C_6(t)$ (see Appendix A).

The previously illustrated sets of parameters were determined through exhaustive experimentation over the proposed PV cell parameter estimation problem and represent the best possible configurations for each of the compared methods [35,36]. Each of the previously mentioned optimization approaches were implemented to solve the minimization problem illustrated by Equation (31). In Table 10, we show the minimization results corresponding to 30 individual runs (with $t = 4000$ iterations each and $N_p = 100$ search agents) for both the SD and DD models, obtained by applying DE, FA, GA, HS, PSO, GSA and CGSA-6. Similarly to the experimental results reported in Section 5.1, the average best, median best and standard deviation of the RMSE values (AB_{RMSE}, MB_{RMSE} and STD_{RMSE}, respectively) were considered as performance indexes when comparing all of the previously mentioned methods. Note once again that the best outcomes for each of the simulated PV cell models are boldfaced.

Table 10. Minimization results for the SD and DD models by applying DE, FA, GA, HS, PSO, GSA and CGSA-6. Each set of results consider 30 individual runs (with $t = 4000$ iterations each and $N_p = 100$ search agents). Note that the best outcomes for each of the simulated solar cell models are boldfaced.

Method	Single-Diode (SD) Model			Double-Diode (DD) Model		
	AB_{RMSE}	MB_{RMSE}	STD_{RMSE}	AB_{RMSE}	MB_{RMSE}	STD_{RMSE}
DE	4.37×10^{-2}	4.77×10^{-2}	6.80×10^{-2}	4.37×10^{-2}	3.77×10^{-2}	2.77×10^{-6}
FA	4.78×10^{-2}	5.79×10^{-2}	6.60×10^{-2}	4.78×10^{-2}	3.92×10^{-2}	5.51×10^{-6}
GA	4.37×10^{-2}	4.77×10^{-2}	6.76×10^{-2}	4.37×10^{-2}	4.77×10^{-3}	4.59×10^{-6}
HS	9.43×10^{-1}	8.27×10^{-1}	6.84×10^{-2}	6.26×10^{-1}	6.53×10^{-1}	7.33×10^{-6}
PSO	4.37×10^{-2}	5.77×10^{-2}	6.91×10^{-2}	4.37×10^{-2}	4.48×10^{-2}	6.42×10^{-6}
GSA	5.27×10^{-2}	5.81×10^{-2}	6.98×10^{-2}	4.04×10^{-1}	3.99×10^{-2}	3.68×10^{-6}
CGSA-6	7.05×10^{-3}	7.32×10^{-3}	6.10×10^{-4}	3.22×10^{-4}	2.63×10^{-4}	1.63×10^{-7}

As expected, when applied to the problem of accurate PV cell parameters estimation, the CGSA-6 algorithm outperforms all of the other methods in both of the proposed model cases (SD and DD). Intuitively, such notable performance is mainly attributed to a better balance between the exploration and exploitation of solutions, which is a direct consequence to the chaotic behaviors incorporated into CGSA-6.

Furthermore, in Figure 14, the evolution curves corresponding to each of the compared methods for both the SD and DD models are shown. As it could be appreciated, the CGSA-6 has both the fastest convergence speed and the property to find much better solutions in comparison to all other of the compared methods. This further demonstrates the superiority of CGSA-6 when applied for the identification of electrical parameters in solar cells. Finally, Tables 11 and 12 show the parameters extracted by each of the compared methods for both the SD model and DD model, respectively. Note that in both cases, the parameters identified by CGSA-6 produce the lowest RMSE values and, as a result, produces the best possible approximation to the I-V characteristics of our implemented solar cell.

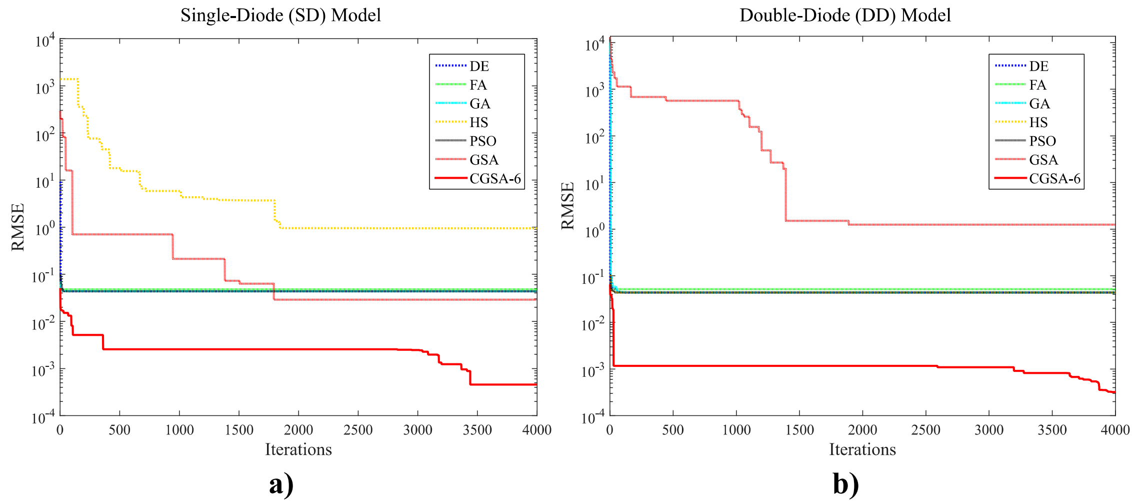

Figure 14. Evolution curves for (**a**) SD Model and (**b**) DD Model, obtained by applying DE, FA, GA, HS, PSO, GSA and CGSA-6.

Table 11. PV cell parameters for the SD model, extracted by applying CGSA-6, DE, FA, GA, HS, PSO and GSA. Note that best RMSE value from among the applied methods is boldfaced.

Parameter	CGSA-6	DE	FA	GA	HS	PSO	GSA
R_s (Ω)	0.0304	0	0	0	0.0170	0	0.0601
R_p (Ω)	65.3951	1.1489	0.8850	1.1650	88.0908	1.1489	10.1123
I_L (A)	0.7891	0.8368	1	0.8329	0.9992	0.8368	0.6653
I_0 (μA)	1.41 $\times 10^{-4}$	0	0	0	2.07 $\times 10^{-2}$	0	0.0451
n	1.9593	1.8923	1	1.8598	1.9983	1	1.9855
RMSE(**X**)	4.57 $\times 10^{-4}$	4.37 $\times 10^{-2}$	4.78 $\times 10^{-2}$	4.37 $\times 10^{-2}$	9.43 $\times 10^{-1}$	4.37 $\times 10^{-2}$	2.88 $\times 10^{-2}$

Table 12. PV cell parameters for the DD model, extracted by applying CGSA-6, DE, FA, GA, HS, PSO and GSA. Note that best RMSE value from among the applied methods is boldfaced.

Parameter	CGSA-6	DE	FA	GA	HS	PSO	GSA
R_s (Ω)	0.0336	0	0	0	0.0072	0	0.0286
R_p (Ω)	60.7589	1.1489	1.0567	1.1586	2.7991	1.1489	59.3050
I_L (A)	0.7613	0.8368	1	0.8344	0.9981	0.8368	0.4865
I_{01} (μA)	2.13 $\times 10^{-9}$	0	0	0	1.12 $\times 10^{-3}$	0	1.29 $\times 10^{-3}$
I_{02} (μA)	5.93 $\times 10^{-7}$	0	0	0	1.42 $\times 10^{-5}$	0	3.59 $\times 10^{-4}$
n_1	1.8872	1.9243	2	1.4022	1.9992	1	1.9894
n_2	1.5459	1	1	1.7970	1.9822	1	1.9420
RMSE(**X**)	3.22 $\times 10^{-4}$	4.37 $\times 10^{-2}$	5.16 $\times 10^{-2}$	4.37 $\times 10^{-2}$	6.26 $\times 10^{-1}$	4.37 $\times 10^{-2}$	2.50 $\times 10^{-1}$

6. Conclusions

In this paper, the population-based optimization approach known as Chaotic Gravitational Search Algorithm (CGSA) [24] was implemented for solving the problem of accurate PV cells parameter identification.

In CGSA, search agents are modeled as masses within a feasible search space (system) whose movement is guided by a set of evolutionary operators inspired in the laws of gravitation and motion. A unique trait of CGSA in comparison to its original counterpart, the Gravitational Search Algorithm (GSA) algorithm [19], is the inclusion of chaotic map functions, embedded into the gravitational motion operators used to define the movement of all masses.

In order to verify the performance of the proposed CGSA-based solar cell parameter estimation approach, a series of comparative experiments against other similar approaches were performed.

As shown by our experimental results, the performance of the proposed CGSA-based parameter identification method easily outperforms all of the other compared approaches. Such a notable performance is mainly attributed to the chaotic behaviors embedded into CGSA, which, as demonstrated by [24], greatly improve the performance by enhancing the exploration and exploitation properties of search agents. The obtained experimental results show that the proposed CGSA-based method is able to accurately extract the unknown electrical parameters which model the behavior of PV cells, and as such, it represents an excellent alternative to tackle such a challenging problem.

Acknowledgments: All sources of funding of the study should be disclosed. Please clearly indicate grants that you have received in support of your research work. Clearly state if you received funds for covering the costs to publish in open access.

Author Contributions: All of the experiments reported in this paper were designed and performed by Arturo Valdivia-Gonzalez, Fernando Fausto and Adrian González. The data and results presented on this work were analyzed and validated by Daniel Zaldívar, Erik Cuevas and Marco Perez-Cisneros. All authors are credited for their contribution on the writing and edition of the presented manuscript.

Conflicts of Interest: The authors declare no conflict of interest.

Appendix A

As illustrated in Section 3, the Chaotic Gravitational Search Algorithm (CGSA) [24] is a modified version to the traditional Gravitational Search Algorithm (GSA) proposed in [19], in which, chaotic behaviors are embedded into the gravitational motion operators which govern the movement of search agents.

Table A1. Chaotic map functions for the proposed CGSA-based PV cell parameter identification approach. The initial value for all of the implemented functions starts at $x_0 = 0.7$

Chaotic Map Function $C_i(t)$	**Math Definition**	**Range (a, b)**
$C_1(t)$ (Chebyshev)	$x_{i+1} = \left(i \cdot \cos^{-1}(x_i)\right)$	$(-1, 1)$
$C_2(t)$ (Circle)	$x_{i+1} = \text{mod}\left(x_i + b - \left(\frac{a}{2\pi}\right)\sin(2\pi \cdot x_i),\ 1\right), \quad a = 0.5,\ b = 0.2$	$(0, 1)$
$C_3(t)$ (Gauss/Mouse)	$x_{i+1} = \begin{cases} 1 & x_i = 0 \\ \frac{1}{\text{mod}(x_i, 1)} & \text{otherwise} \end{cases}$	$(0, 1)$
$C_4(t)$ (Iterative)	$x_{i+1} = \sin\left(\frac{a \cdot \pi}{x_i}\right), \quad a = 0.7$	$(0, 1)$
$C_5(t)$. (Logistic)	$x_{i+1} = a \cdot x_i(1 - x_i), \quad a = 4$	$(-1, 1)$
$C_6(t)$ (Piecewise)	$x_{i+1} = \begin{cases} \frac{x_i}{P} & 0 \le x_i < P \\ \frac{X_i - P}{0.5 - P} & P \le x_i < 0.5 \\ \frac{1 - P - x_i}{0.5 - P} & 0.5 \le x_i < 1 - P \\ \frac{1 - x_i}{P} & 1 - P \le x_i < 1 \end{cases} \quad P = 0.4$	$(0, 1)$
$C_7(t)$ (Sine)	$x_{i+1} = \frac{a}{4}\sin(\pi \cdot x_i), \quad a = 4$	$(0, 1)$
$C_8(t)$ (Singer)	$x_{i+1} = \mu\left(7.86x_i - 23.31x_i^2 + 28.75x_i^3 - 13.302875x_i^4\right), \quad \mu = 2.3$	$(0, 1)$
$C_9(t)$ (Sinusoidal)	$x_{i+1} = a \cdot x_i^2 \sin(\pi \cdot x_i), \quad a = 2.3$	$(0, 1)$
$C_{10}(t)$ (Tent)	$x_{i+1} = \begin{cases} \frac{x_i}{0.7} & x_i < 0.7 \\ \frac{10}{3}(1 - x_i) & x_i \ge 0.7 \end{cases}$	$(0, 1)$

As explained in Section 3.2, such chaotic behaviors are modeled by a particular chaotic map function $C_i(t)$, which is further normalized into a given adaptive interval. For the experiments reported in this paper, we compared the performance of CGSA with regard to 10 different chaotic map functions. In Table A1, the detailed list of all of the implemented chaotic maps is shown.

References

1. Yuan, X.; He, Y.; Liu, L. Parameter extraction of solar cell models using chaotic asexual reproduction optimization. *Neural Comput. Appl.* **2015**, *26*, 1227–1239. [CrossRef]

2. Oliva, D.; Cuevas, E.; Pajares, G. Parameter identification of solar cells using artificial bee colony optimization. *Energy* **2014**, *72*, 93–102. [CrossRef]
3. Jamadi, M.; Mehdi, F.M. Very accurate parameter estimation of single- and double-diode solar cell models using a modified artificial bee colony algorithm. *Int. J. Energy Environ. Eng.* **2015**, *7*, 13–25. [CrossRef]
4. Emery, K. Measurement and Characterization of Solar Cells and Modules. In *Handbook of Photovoltaic Science and Engineering*; John Wiley & Sons, Ltd.: Hoboken, NJ, USA, 2003; pp. 701–752.
5. Sarkar, M.N.I. Effect of various model parameters on solar photovoltaic cell simulation: A SPICE analysis. *Renew. Wind Water Sol.* **2016**, *3*, 13. [CrossRef]
6. Humada, A.M.; Hojabri, M.; Mekhilef, S.; Hamada, H.M. Solar cell parameters extraction based on single and double-diode models: A review. *Renew. Sustain. Energy Rev.* **2016**, *56*, 494–509. [CrossRef]
7. El Tayyan, A.A. An approach to extract the parameters of solar cells from their illuminated I-V curves using the Lambert W function. *Turk. J. Phys.* **2015**, *39*, 1–15. [CrossRef]
8. Han, W.; Wang, H.; Chen, L. Parameters Identification for Photovoltaic Module Based on an Improved Artificial Fish Swarm Algorithm. *Sci. World J.* **2014**, *2014*, 859239. [CrossRef] [PubMed]
9. Chen, Z.; Wu, L.; Lin, P.; Wu, Y.; Cheng, S. Parameters identification of photovoltaic models using hybrid adaptive Nelder-Mead simplex algorithm based on eagle strategy. *Appl. Energy* **2016**, *182*, 47–57. [CrossRef]
10. Tamrakar, R.; Gupta, A. Extraction of Solar Cell Modelling Parameters Using Differential Evolution Algorithm. *Int. J. Innov. Res. Electr. Electr. Instrum. Control Eng.* **2015**, *3*, 78–82. [CrossRef]
11. Yoon, Y.; Geem, Z.W. Parameter Optimization of Single-Diode Model of Photovoltaic Cell Using Memetic Algorithm. *Int. J. Photoenergy* **2015**, *2015*, 963562. [CrossRef]
12. Zhang, Y.; Lin, P.; Chen, Z.; Cheng, S. A Population Classification Evolution Algorithm for the Parameter Extraction of Solar Cell Models. *Int. J. Photoenergy* **2016**, *2016*, 2174573. [CrossRef]
13. Marini, F.; Walczak, B. Chemometrics and Intelligent Laboratory Systems Particle swarm optimization (PSO). A tutorial. *Chemom. Intell. Lab. Syst.* **2015**, *149*, 153–165. [CrossRef]
14. Karaboga, D.; Basturk, B. On the performance of artificial bee colony (ABC) algorithm. *Appl. Soft Comput.* **2008**, *8*, 687–697. [CrossRef]
15. Beyer, H.G.; Schwefel, H.P.; Wegener, I. How to analyse evolutionary algorithms. *Theor. Comput. Sci.* **2002**, *287*, 101–130. [CrossRef]
16. Storn, R.; Price, K. Differential Evolution—A Simple and Efficient Heuristic for global Optimization over Continuous Spaces. *J. Glob. Optim.* **1997**, *11*, 341–359. [CrossRef]
17. Kirkpatrick, S.; Gelatt, C.D.; Vecch, M.P. Optimization by Simulated Annealing. *Science* **2007**, *220*, 671–680. [CrossRef] [PubMed]
18. Geem, Z.; Kim, J.; Loganathan, G.V. A New Heuristic Optimization Algorithm: Harmony Search. *Simulation* **2001**, *76*, 60–68. [CrossRef]
19. Rashedi, E.; Nezamabadi-pour, H.; Saryazdi, S. GSA: A Gravitational Search Algorithm. *Inf. Sci. (NY)* **2009**, *179*, 2232–2248. [CrossRef]
20. Sarjila, R.; Ravi, K.; Edward, J.B.; Kumar, K.S.; Prasad, A. Parameter Extraction of Solar Photovoltaic Modules Using Gravitational Search Algorithm. *J. Electr. Comput. Eng.* **2016**, *2016*, 2143572. [CrossRef]
21. Baykasoğlu, A.; Ozsoydan, F.B. Adaptive firefly algorithm with chaos for mechanical design optimization problems. *Appl. Soft Comput.* **2015**, *36*, 152–164. [CrossRef]
22. Yang, D.; Liu, Z.; Zhou, J. Chaos optimization algorithms based on chaotic maps with different probability distribution and search speed for global optimization. *Commun. Nonlinear Sci. Numer. Simul.* **2014**, *19*, 1229–1246. [CrossRef]
23. Liu, B.; Wang, L.; Jin, Y.-Y.H.; Huang, D.-X.; Liu, L.W.B.; Tang, F. Improved particle swarm optimization combined with chaos. *Chaos Solitons Fractals* **2005**, *25*, 1261–1271. [CrossRef]
24. Mirjalili, S.; Gandomi, A.H. Chaotic Gravitational Constants for The Gravitational Search Algorithm. *Appl. Soft Comput.* **2017**, *53*, 407–419. [CrossRef]
25. Chatterjee, A.; Roy, K.; Chatterjee, D. A Gravitational Search Algorithm (GSA) based Photo-Voltaic (PV) excitation control strategy for single phase operation of three phase wind-turbine coupled induction generator. *Energy* **2014**, *74*, 707–718. [CrossRef]
26. Jiang, S.; Wang, Y.; Ji, Z. A new design method for adaptive IIR system identification using hybrid particle swarm optimization and gravitational search algorithm. *Nonlinear Dyn.* **2015**, *79*, 2553–2576. [CrossRef]

27. Chakraborti, T.; Chatterjee, A. A novel binary adaptive weight GSA based feature selection for face recognition using local gradient patterns, modified census transform, and local binary patterns. *Eng. Appl. Artif. Intell.* **2014**, *33*, 80–90. [CrossRef]
28. Jamshidi, Y.; Kaburlasos, V.G. GsaINknn: A GSA optimized, lattice computing knn classifier. *Eng. Appl. Artif. Intell.* **2014**, *35*, 277–285. [CrossRef]
29. Shukla, A.; Singh, S.N. Multi-Objective Unit Commitment With Renewable Energy Using GSA Algorithm. *INAE Lett.* **2016**, *1*, 21–27. [CrossRef]
30. Easwarakhanthan, T.; Bottin, J.; Bouhouch, I.; Boutrit, C. Nonlinear Minimization Algorithm for Determining the Solar Cell Parameters with Microcomputers. *Int. J. Sol. Energy* **1986**, *4*, 1–12. [CrossRef]
31. Ma, J.; Ting, T.O.; Man, K.L.; Zhang, N.; Guan, S.U.; Wong, P.W.H. Parameter estimation of photovoltaic models via cuckoo search. *J. Appl. Math.* **2013**, *2013*, 10–12. [CrossRef]
32. Dubey, S.; Sarvaiya, J.N.; Seshadri, B. Temperature dependent photovoltaic (PV) efficiency and its effect on PV production in the world—A review. *Energy Procedia* **2013**, *33*, 311–321. [CrossRef]
33. Gao, X.Z.; Govindasamy, V.; Xu, H.; Wang, X.; Zenger, K. Harmony Search Method: Theory and Applications. *Comput. Intell. Neurosci.* **2015**, *2015*, 258491. [CrossRef] [PubMed]
34. Yang, X. Firefly Algorithm, Lévy Flights and Global Optimization. *Res. Dev. Intell. Syst. XXVI* **2010**, 209–218. [CrossRef]
35. Awadallah, M.A.; Venkatesh, B.; Member, S. Bacterial Foraging Algorithm Guided by Particle Swarm Optimization for Parameter Identification of Photovoltaic Modules Algorithme de recherche de nourriture bactérienne guidé par l' optimisation par essaims particulaires pour l' identification de param. *Can. J. Electr. Comput. Eng.* **2016**, *39*, 150–157. [CrossRef]
36. Awadallah, M.A. Variations of the bacterial foraging algorithm for the extraction of PV module parameters from nameplate data. *Energy Convers. Manag.* **2016**, *113*, 312–320. [CrossRef]